Deformation Mechanisms of Polymer Thin Films by Simultaneous Kinetic Measurement of Microscopic Infrared Dichroism and Macroscopic Stress. 2. Molecular Orientation during Necking Process of Isotactic Polypropylene

Yihu Song,[†] Koh-hei Nitta,[‡] and Norio Nemoto*,[†]

Department of Molecular and Material Sciences, IGSES, Kyushu University, Hakozaki, Fukuoka 812-8581, Japan, and School of Materials Science, Japan Advanced Institute of Science and Technology, Ishikawa 923-1292, Japan

Received September 3, 2002; Revised Manuscript Received November 26, 2002

ABSTRACT: The molecular orientations in the crystalline and the amorphous phases in a quenched isotactic polypropylene (iPP) film with a smectic structure are studied using an instrument constructed for simultaneous kinetic measurement of microscopic infrared (MicIR) dichroism from a predetermined sampling area with a size of 200 × 200 μm^2 and macroscopic stress of film uniaxially stretched at a constant elongation rate at 30 °C. Local deformation behavior in the sampling area is determined for one sample using a method of photogrammetry. During the passage of the necking through the sampling area, the local extension ratio $\lambda(t)$ increases fast from 1.5 to 5, which induces the rapid orientation of iPP chains in both the crystalline and the amorphous phases. The orientation function of the amorphous phase, f_{am}, from the mesoscale deformation of the sampling area is found to be well described by the pseudo-affine deformation mechanism, since the local area shrinks anisotropically during the passage of the neck shoulder. The orientation function f_c in the crystalline phase increases linearly with f_{am} up to $f_{am} = 0.3$ with a slope of 1.85 for all samples tested. In the neck entity, the crystal orientation may lag behind the amorphous chain orientation due to the enhanced plastic deformations. It is shown that the behavior of the amorphous phase is essential for the averaged lamellar orientation on the mesoscale.

Introduction

Scientific interest in the plastic deformation of semicrystalline polymers has made considerable progress in understanding the yielding and the necking phenomena in relation to the macroscopic mechanical behavior and the microscopic structural evolution.[1−24] Semianalytical and numerical approaches to the macroscopic mechanical behaviors have also been developed in order to clarify the deformation mechanism.[25−28] It is realized only recently that the macroscopic stress−strain curves do not provide any correct description of the inhomogeneous deformation with a neck propagation, which requires the measurement of both the true stress and the true strain in local terms.[29−31]

The necking behavior can be qualitatively disclosed from the macroscopic strain dependence of infrared dichroism using traditional Fourier transform infrared (FT-IR) spectroscopy.[32−35] However, it is not clear yet how molecules, especially the constrained amorphous chains, behave through the necking process except for the qualitative understanding that different processes such as onset of isolated crystallite slip, cooperation of the slips, crystallite fragmentation, and amorphous chain disentanglement may be involved as strain is increased.[24,25]

In our laboratory, equipment for simultaneous kinetic measurement of microscopic infrared (MicIR) dichroism from a predetermined small sampling area and macroscopic stress of a polymer thin film subjected to uniaxial stretching at a constant elongation rate has been constructed,[36] which has been used for studying the deformation mechanism of isotactic polypropylene (iPP) thin films with various morphologies.[37] We have found that the MicIR dichroism does not show any definite relationship with the macroscopic mechanical behavior of iPP films, which leads to supposition that the molecular orientation should be studied in relation to the actual local deformation induced by the passage of the necking through the sampling area.[37] To interpret the underlying molecular ground of the necking on a mesoscale, we in this paper apply a convenient method for in-situ simultaneous measurement of the molecular orientation and the local deformation within a single sampling area with a size of 200 × 200 μm^2 in an iPP film. This size of the sampling area is not the lowest limit of our equipment but is chosen for the measurement of local strain by proper selection of internal references. The deformation mechanism in the macroscopic plastic deformation region and the relationship between the molecular orientations of the crystalline and the amorphous phases shall be discussed in detail. Special attention will be paid to the deformation mode of the constrained amorphous chains on the mesoscale of 200 μm.

Experimental Section

Materials. The preparation of the quenched iPP thin film with a smectic structure was described in an earlier paper.[37] Crystal-like domains with irregular shapes and with a size from several microns to several decades of micron were found to be considerably abundant in this film, which may be the aggregates of the defective α-crystals.[38−42] One of the crystal aggregates was carefully chosen in the film center before elongation as a mark of the sampling area to which the microscopic infrared (MicIR) dichroism was sampled. Only data from the samples with a reference crystal aggregate distinguishable up to the end of stretching were analyzed.

[†] Kyushu University.
[‡] Japan Advanced Institute of Science and Technology.
* To whom correspondence should be addressed. E-mail: nemo@mm.kyushu-u.ac.jp.

10.1021/ma0214254 CCC: $25.00 © 2003 American Chemical Society
Published on Web 02/21/2003

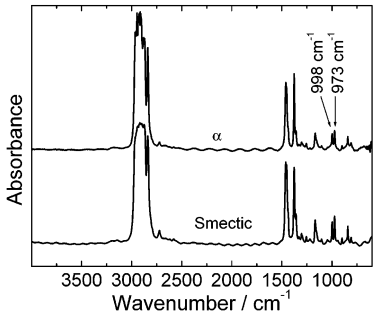

Figure 1. MicIR spectra for the quenched and the annealed iPP films with the smectic and the α-monoclinic structures, respectively.

The MicIR spectrum of the quenched film is given in Figure 1 together with the spectrum of another film annealed at 145 °C for 4 h and containing the α-spherulites. The MicIR spectra of the two films are essentially the same because of their same primary 3_1 helical structure. In an IR dichroism study, the quenched film can be considered as being composed of two phases, i.e., the crystalline and the amorphous phases.[35]

Apparatus. The setup details of the equipment were described in an earlier paper.[36] The equipment permits simultaneous kinetic measurement of macroscopic nominal stress σ and MicIR dichroism from a small sampling area during uniaxial stretching of a thin film at a constant elongation rate. We describe the principle here in brief in consideration that this equipment provides a new type of measurement of the IR dichroism using the kinetic scan mode. The IR light beam was provided by the FTS 6000 spectrometer (Bio-Rad). After passing through a polarizer and a photoelastic modulator (PEM-90 ZnSe, Hinds Instruments) successively, the beam was irradiated vertically on the film sample from the bottom. The transmitted light was detected using a mercury−cadmium−telluride (MCT) detector installed on an infrared microscope of UMA 500 (Bio-Rad). By setting the peak retardation of the modulator as the half-wave, the transmitted light was divided into a broad-band signal of $AC(t) = A_{\parallel}(t) - A_{\perp}(t)$ and a low pass signal of $DC(t) = A_{\parallel}(t) + A_{\perp}(t)$. Here $A_{\parallel}(t)$ and $A_{\perp}(t)$ are the polarized spectra at stretching time t with the IR radiation parallel and perpendicular to the draw axis, respectively. After passing through a lock-in amplifier (LIA SR510, Stanford Co.) and a ratio circuit, the $AC(t)$ and the $DC(t)$ outputs were changed to analogue voltages and were alternatively sampled in a computer with a sampling interval of about 30 s. Intensities of the desired peaks in the $AC(t)$ and the $DC(t)$ spectra were evaluated in terms of peak height, which resulted in the dichroism data reliable to the same extent as those from the direct measurement of the $A_{\parallel}(t)$ and the $A_{\perp}(t)$ spectra during elongation.[37] The reliability of the kinetic scan mode was also verified by comparing our data with the earlier data reported by Siesler.[37,43]

The sample cell of the elongation device was mounted in the same compartment of the FT-IR system. The infrared or visible beam was irradiated directly on the film, which allowed us to sample the infrared signal or to observe the sampling area by switching the view/detection selection optics on the IR microscope. Because of the low elongation speed as well as the synchronized movement of the two clamps, we were able to adjust the reference crystal aggregate to the fixed laboratory coordinates under the desired viewing field by moving the $x-y-z$ stage at a time interval of 3 min whenever the sampling area did not stay in its original position. From this adjustment, the displacement of the sampling area relative to the film center along the draw axis, $D_L(t)$, was recorded and used to characterize the influence of the inhomogeneous deformation on the molecular orientation in the sampling area. To make it simple for comparison of individual specimens, the measured $D_L(t)$ is multiplied by -1 or $+1$ depending on its sign so that its value at the earlier stage of elongation may become always positive.

The displacement of the sampling area during elongation could not be avoided due to the inhomogeneous deformation including the necking phenomenon, which was the reason that we used the low stretching speed in this study. When the sampling area is located outside the neck and also after it enters the neck entity, deformation in these two sections becomes small. Therefore, fast displacement of the sampling area may bring about essentially negligible influences on $AC(t)$ and $DC(t)$ values. The most important deformation and molecular orientation occur at the neck shoulder when the neck is passing through the sampling area. At this stage, the moving speed of the sampling area drastically decreases to a small finite value. An average displacement speed was estimated as ca. 15 μm min^{-1}. Since a small portion of the material present in the sampling area is moved out during the measurement time of 30 s, the sampled MicIR dichroism reflects, strictly speaking, the molecular orientation in the close vicinity of the desired area, but use of the sampling area with the length as large as 200 μm along the draw axis hardly influences main results given below.

Method. The film was cut to rectangular-shaped specimens with a size of 10 × 3 mm^2 (length × width), which was fastened between the two clamps and stretched at 30.0 ± 0.1 °C with a constant elongation rate of $\dot{\epsilon} = V_E/L_0 = 0.066$ min^{-1}. Here, V_E and L_0 are the stretching speed and the initial film length between the two clamps, respectively. The viewing field for sampling of the MicIR dichroism signal was 200 × 200 μm^2 in this study. The parameters of the spectrometer were the same as described in an earlier paper.[37]

A method of photogrammetry was employed for in-situ determination of the local strain within the sampling area to one sample. A digital camera (Camedia C4040Z00M, Olympus Optical Co. Ltd.) equipped with a microscope lens was connected with the ocular of the IR microscope, and micrographs of the sampling area were recorded at selected time t during elongation. Distances between four crystal aggregates in the sampling area were read from the micrographs in order to evaluate the actual deformation in the length−width plane of the film.

In the kinetic scan, the Hermans orientation function for a particular absorption band can be derived as

$$f = \frac{2A(t)}{3 - A(t)} \frac{R_0 + 2}{R_0 - 1} \tag{1}$$

where $R_0 = 2\cot^2\psi$ is the perfect dichroic ratio of a transition moment making an angle ψ with the direction of the molecular main chain axis and $A(t) = AC(t)/DC(t)$. The orientation function of the crystalline phase, f_c, was determined from the 998 cm^{-1} band.[43] The orientation function of the amorphous phase, f_{am}, was calculated from the 973 and 998 cm^{-1} bands based on a two-phase model.[44,45] The π-band at 973 cm^{-1} belongs to the CH_3 rocking and the axial and equatorial C−C stretching modes in both the amorphous and the crystalline phases, while the π-band at 998 cm^{-1} involves the CH_3 rocking, the C−CH_3 stretching, the CH bending, and the CH_2 twisting modes in the crystalline phase.[43−45]

Results

Time Profiles of *AC*(*t*) and *DC*(*t*) Spectra. Typical examples of the $AC(t)$ and the $DC(t)$ spectra in the 1040−940 cm^{-1} region recorded at various stretching times t are shown in Figure 2. Peak intensities of the $AC(t)$ spectra increase while those of the $DC(t)$ spectra decrease with the local extension in the sampling area, which reflect an increase in molecular orientation and a reduction in film thickness, respectively. The $AC(t)$ spectra suggest a slightly perpendicular orientation of main-chain axis in advance of the significant parallel orientation, being consistent with the earlier findings.[34,43]

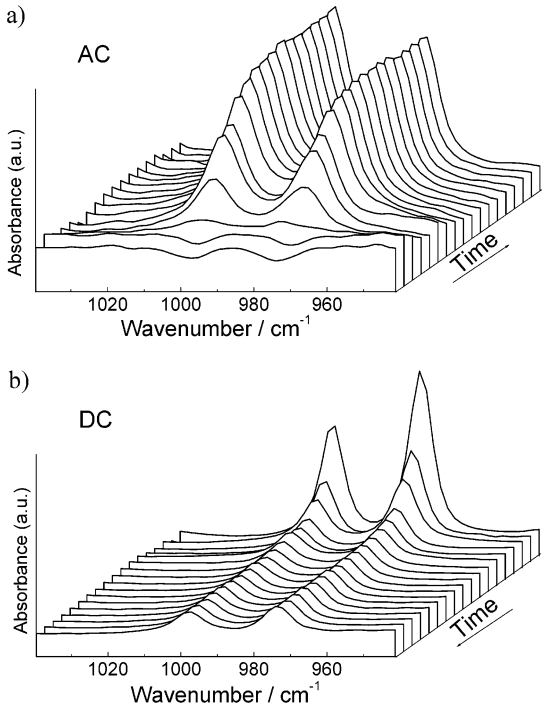

Figure 2. Changes in $AC(t)$ and $DC(t)$ spectra of an iPP film in the 1040−940 cm^{-1} wavenumber region as the sample is uniaxially stretched.

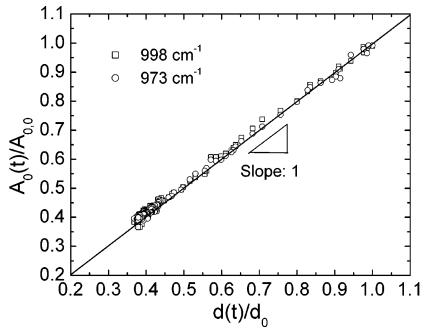

Figure 3. Linear relationship between the structural absorbances of the 998 and 973 cm^{-1} bands and the film thickness estimated from the interference pattern in the $DC(t)$ spectra.

Structural Absorbance. The structural absorbance $A_0(t)$, which is quite of importance in IR dichroism studies, can be evaluated through

$$A_0(t) = \frac{A_{\parallel}(t) + 2A_{\perp}(t)}{3} = \frac{DC(t)}{2} - \frac{AC(t)}{6} \qquad (2)$$

In Figure 3, the relative structural absorbances $A_0(t)/A_{0,0}$ of the 973 and 998 cm^{-1} bands are shown to be linearly dependent on the relative film thickness $d(t)/d_0$ estimated from the interference pattern in the $DC(t)$ spectra.[36] Here $A_{0,0}$ ($\equiv A_0(0)$) and d_0 ($\equiv d(0)$) are the structural absorbance and the film thickness before elongation, and $d(t)$ is the film thickness at the stretching time t. The linear relationship with a slope of unity indicates that the two bands are involved in a change in film thickness, irrespective of the microstructure. The result offers a convenient method for directly pursuing the thickness of the small sampling area.

Influence of Necking Propagation on Time Profiles of σ, f_c, f_{am}, and $D_L(t)$. Parts a, b, and c of Figure 4 show the time profiles of the nominal stress σ, the orientation functions f_c and f_{am}, and the displacement

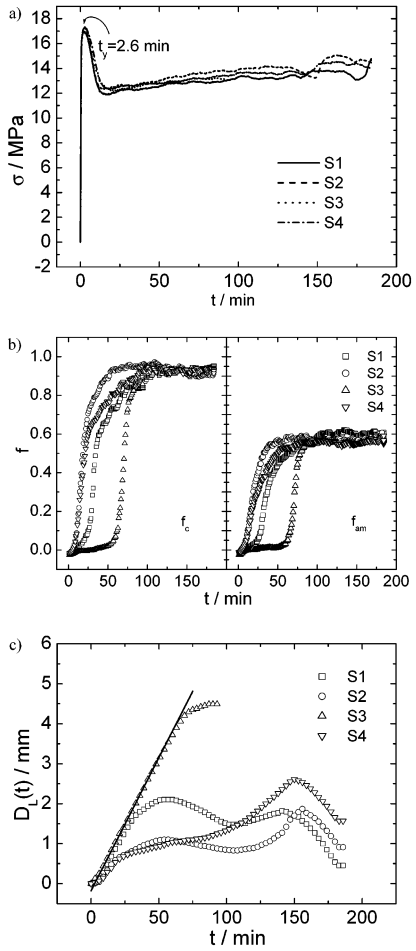

Figure 4. Time profiles of the macroscopic stress σ (a), the microscopic orientation functions f_c and f_{am} (b), and the displacement of the sampling area $D_L(t)$ (c) from four specimens S1, S2, S3, and S4 with $L_0 = 2$ mm. Before the sampling area suffers from the necking, the $D_L(t)$ data of S3 are found to be located on the straight line given by $D_L(t) = (t - t_y)V_E/2$.

of the sampling area $D_L(t)$, respectively, from four specimens with $L_0 = 2$ mm. The σ profiles follow the general characteristic of the uniaxial deformation although slight differences are observed even before the yielding point (t_y) is reached. Great differences in the MicIR dichroism profiles among the four samples are clearly seen in Figure 4b, which show the inhomogeneous deformation on the mesoscale of 200 μm. In fact, the inhomogeneous deformation dominated by a neck initiation and propagation directly results in an unpredictable molecular orientation in the sampling area as a function of time t, but this is not the case for the σ profile.

The time profiles of $D_L(t)$ in Figure 4c also appear to vary from one sample to another. The $D_L(t)$ remains essentially zero to an experimental accuracy until t_y is reached and then starts to increase linearly with the slope of $V_E/2$ as evidenced by the close fit of the data for the sample S3 to the straight line calculated from $D_L(t) = (t - t_y)V_E/2$ in the figure. It is to be noted that the deviation of $D_L(t)$ from the straight line occurs at around the stretching time where f_{am} and f_c start to increase rapidly. The behaviors become quite complicated at longer t.

Combining the MicIR dichroism and the $D_L(t)$ profiles of the sample S3, it is likely that the deformation outside the neck is negligible in comparison with that

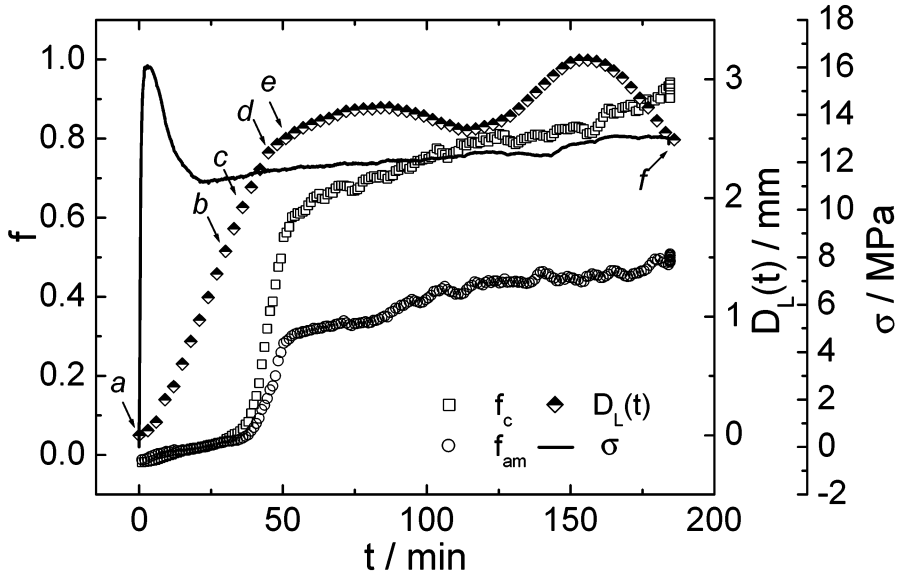

Figure 5. Time profiles of σ, f_c, and f_{am} as well as $D_L(t)$ from a specimen S8 with $L_0 = 2$ mm.

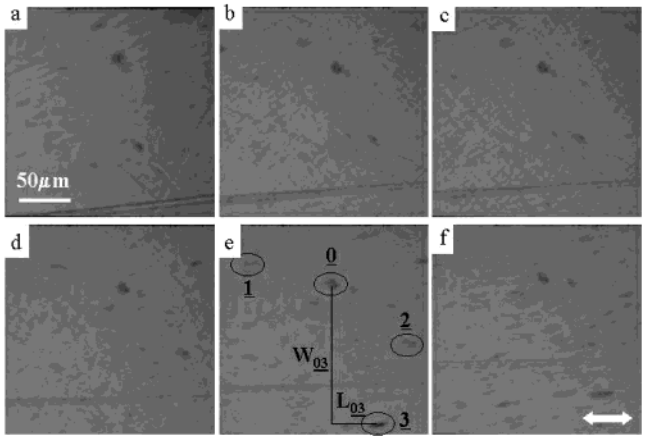

Figure 6. Morphology evolution of the sampling area in the specimen S8 during continuous uniaxial elongation. The heavy arrow shows the draw axis, and the micrograph serial numbers are marked in Figure 5.

at the neck shoulder. The onset of the molecular orientation is clearly linked with the deviation of $D_L(t)$ from its initial linear portion when the sampling area touches the neck shoulder. After the sampling area leaves the neck shoulder and enters the neck entity, molecules finally reach a highly oriented state with $f_c = 0.94 \pm 0.04$ and $f_{am} = 0.57 \pm 0.05$, which look to depend on the resistance of the local area to the necking.

The same kind of measurement was also performed to other three specimens S5, S6, and S7 with $L_0 = 0.5$, 1, and 2 mm, respectively. Although the macroscopic mechanical behavior varies due to a change in L_0, the rapid molecular orientation begins only when the $D_L(t)$ starts to depart from its initially linear portion, the same as the results in Figure 4.

Morphology Evolution Accompanying Molecular Orientation. Figure 5 shows the time profiles of σ, f_c, and f_{am}, as well as $D_L(t)$ from a specimen S8 with $L_0 = 2$ mm, to which many in-situ micrographs of the sampling area were taken and are selectively shown in Figure 6. The morphology changes slightly according to the apparent homogeneous deformation in the vicinity of the sampling area while it is located outside the neck and in the neck entity. During the necking passage through the sampling area, distances of the crystal aggregates distinguishable under the IR microscope rapidly increase along the draw direction, indicating that a dramatic deformation occurs at the neck shoulder. A portion of the crystal aggregates is occasionally partially destroyed to small pieces due to the deformation of amorphous chains linking the crystallites. On the other hand, some of the crystal aggregates are mechanically stable to resist the necking to some extent. No flow occurs during the drawing process.

Local Deformation. Measuring changes in distances of three crystal aggregate pairs 0−1, 0−2, and 0−3 in the micrographs of the sampling area as denoted in photograph e of Figure 6, the local extension ratio along the draw axis, $\lambda(t)$, and the relative shrinkage along the film width direction, $W(t)/W_0$, were determined for specimen S8. The results are given in Figure 7 together with $d(t)/d_0$ estimated from $A_0(t)/A_{0,0}$. The film shrinks equally in the thickness and the width directions before the sampling area suffers from necking where a slight molecular orientation (Figure 5) together with a slow local extension (Figure 7b) is detected. Beyond about $t = 37$ min when the sampling area touches the neck shoulder, the dramatic molecular orientation and longitudinal extension start. Above $\lambda(t) \sim 1.8$, eventually, shrinkage in width lags behind that in thickness, which appears as a general characteristic of the necking in iPP thin films due to the different normal stresses established along the neck shoulder.[37] A simple calculation shows that Poisson's ratio ν is located in the range 0.45−0.50 in the whole deformation, being contrary to the well-accepted value of $\nu = 0.3$.[46,47] This result shows that the deformation is not accompanied by a marked volume change, and the iPP sample may be considered to behave as an incompressible material during the local deformation in the neck shoulder to good approximation.

Discussion

Molecular Orientation in the Amorphous Phase. The deformation looks inhomogeneous even in the mesoscale of 200 μm order because of the existence of less deformed crystal aggregates embedded in a highly deformed surrounding microcrystalline region. It is also true that the dominant molecular orientation has been induced by the local deformation in the close vicinity of the sampling area during the passage of the neck

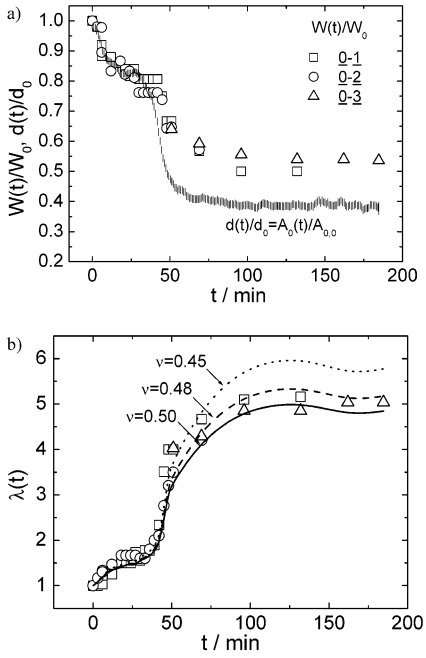

Figure 7. Local deformations in film width (a) and length L_{0i} (i = 1, 2, and 3) along the draw axis (b) read from the changes in distances between the crystal aggregate pairs 0−1, 0−2, and 0−3 in the micrographs of the sampling area from the specimen S8. The relative film thickness $d(t)/d_0$ estimated from $A_0(t)/A_{0,0}$ is given in (a) together with the relative width, $W(t)/W_0 = W_{0i}(t)/W_{0i}(t{=}0)$. The local extension ratio is estimated from $\lambda(t) = L_{0i}(t)/L_{0i}(t{=}0)$. The curves in (b) show the results calculated from $\lambda(t) = \{W(t)d(t)/W_0d_0\}^{-1/2\nu}$ with selected values of the logarithmic Poisson's ratio ν.

shoulder. The MicIR dichroism originates from the averaged orientation of molecules from the local area with a size as yet much larger than a contour length of the iPP molecule. Thus, it seems worthy of an attempt to look into a relationship between the orientation function related to the averaged molecular orientation and the local strain measured on a mesoscopic scale. In consideration that the constrained amorphous iPP chains are in the rubbery state at 30 °C higher than its glass transition temperature and the lengths of amorphous chains are many times greater than the lamellar thickness, we may be allowed to make an attempt to deal with the orientation of amorphous chains within the framework of rubber elasticity.

The orientation function of a rubber network upon uniaxial stretching is related to the network parameters and the deformation by[48−52]

$$f = C\{\lambda(t)^2 - \lambda(t)^{-1}\} \qquad (3)$$

whenever the network chains deform affinely. Here the front factor C depends on the choice of the detailed molecular model, e.g., $C = 1/(5N_k)$ in the Kuhn expression with N_k the average number of freely jointed Kuhn segments between cross-linking points.[48,49] When chains within a rubber matrix experience an anisotropic mean field through their excluded-volume interactions, C is given as $C = b/15\pi N_g\xi$, where ξ is the Edwards' screening length and N_g the number of Gaussian statistical segments with an average size b between the junctions.[52]

f_{am} in Figure 5 is replotted against $\lambda(t)$ in Figure 8. Rather surprisingly, we find that a change in f_{am} against $\lambda(t)$ for $\lambda(t) < 4.5$ can be well described by eq 3 with C = 0.018 or N_k = 11. This strongly suggests that the amorphous phase deforms affinely on a mesoscale within the experimental error for some time interval of deformation. The f_{am} seems to deviate from the prediction of the affine deformation beyond $\lambda \simeq 5$. It might be better to call such a particular deformation of amorphous chains as a pseudo-affine deformation on the mesoscale in consideration that f_{am} does not show any definite relationship with the macroscopic extension of film that shrinks unequally in the width and the thickness directions. It seems reasonable to consider that N_k is dependent on the size of a detectable local area as well as its morphology and the degree of crystallinity.

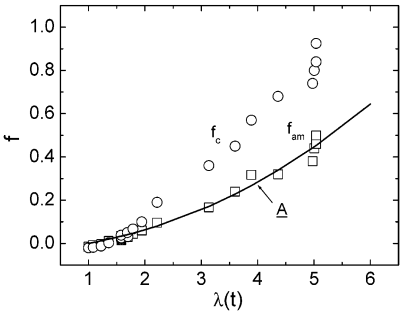

Figure 8. Molecular orientation functions f_c and f_{am} as a function of $\lambda(t)$ for the specimen S8. Curve A gives the theoretical prediction from the model of the affine deformation of rubber network.

The pseudo-affine deformation of iPP film on a mesoscale is completely different from the affine deformation of true elastomers in which the isotropic shrinkage is always satisfied independent of the observation scale. One may notice that the isotropic shrinkage occurs in the film width and thickness directions at t < 37 min (Figure 7) corresponding to f_{am} < 0.07 (Figure 5) for the sample S8. The material present outside the neck may deform following the true affine deformation mode. The deformation turns into the pseudo-affine mode during the necking that accelerates the local deformation at the neck shoulder. Despite the geometrical complexity of the necking, the agreement between the experimental data and the theoretical prediction of eq 3 suggests that the averaged molecular orientation of the amorphous phase is directly related to the longitudinal extension of the local area.

The plastic deformation on the lamellar level affects several deformation mechanisms of the crystalline and the amorphous components.[53] Besides the important crystallographic slip of crystallites, two basic modes of interlamellar sliding (shear) and lamellar separation (extension) are known to have a close relationship with the deformation of amorphous chains.[54,55] The interlamellar sliding proceeds primarily at the early stage of deformation, resulting in the necking initiation. The further molecular orientation within the thin amorphous layers along with the neck propagation is then constrained by the adjacent lamellae that possess a modulus much higher than that of the amorphous component and operate as multifunctional cross-links.[56−60] On the basis of these ideas, we consider that the ideal rubberlike behavior in the amorphous phase may lead to the lamellar separation as a local area is moved along the neck shoulder, if the lamellar fragmentation or microcracking does not occur markedly.

Relationship between f_c and f_{am}. A plot of f_c against f_{am} in Figure 9 reveals a linear relationship with

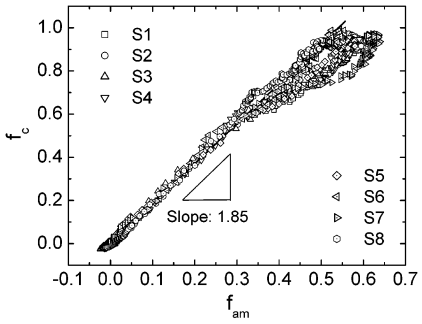

Figure 9. Relationship between f_c and f_{am} for eight specimens.

a slope of 1.85 up to $f_{am} \approx 0.3$ about a half of the final value $f_{am} \approx 0.57 \pm 0.05$ after the necking passage. If the chain extensibility is not exhausted, further chain deformation can occur after the sampling area enters the neck entity though the molecular orientation is decelerated, as shown in Figure 5. In some cases, nevertheless, the linear relationship may extend approximately to $f_{am} = 0.5$, covering almost the whole range of deformation tested. The straightforward linear relationship suggests that the lamellar orientation is simply determined by the deformation of the surrounding amorphous chains at the earlier stage of the necking propagation through the sampling area, independent of the initial size of the sample, the initial necking position, and the necking propagation speed. It appears that a large population of lamella is not destructed during the dramatic deformation at the neck shoulder. It is likely that sheared lamellae are rotated alongside with the lamellar translation and that the plastic deformations are not yet so significant on the mesoscale as to influence the deformation of amorphous chains and the orientation of lamellae.

The large data scattering of f_c aganist f_{am} at $f_{am} > 0.3$ implies that really complicated multiple processes are involved in the deformation and the orientation of the crystalline phase on the observation scale. The MicIR dichroism data without those obtained by another type of measurement such as X-ray diffractometry provide a reliable method neither for judging which contribution is dominative nor for elucidating its relationship with amorphous chain deformation. At $0.3 < f_{am} < 0.5$, the crystal orientation becomes slower than the amorphous chain orientation. At the later stage of deformation at $f_{am} > 0.5-0.6$, on the other hand, the slope of f_c against f_{am} increases again, which might be responsible for the fibrillation[61] and the stress-induced crystallization and decrystallization.[62]

f_c as a function of $\lambda(t)$, as shown in Figure 8, gives a description of the orientation of the special flakelet-like lamellar cross-links in the rubbery network of amorphous chain. The models of the uniform[63] and the affine or the pseudo-affine[48,64,65] deformation of spherulite were found to be successful in explanation of the crystal orientation in a carefully stretched polyethylene film free of necking[63,66] and an iPP film deformed at 110 °C,[67] but none of them is applicable for describing our result from the iPP film with a smectic but not a spherulitic structure and stretched at room temperature. The present work may request an essentially new type of theoretical formulation for explanation of inhomogeneous deformation of semicrystalline polymers, taking into consideration the cooperation between the crystalline and the amorphous phases alongside with their respective contributions at various levels.

Plastic deformations of crystal on the nanometer scale do not prevent the cold drawing of the iPP film with a smectic structure markedly. Needless to say, the deformation of amorphous chains strongly contributes to the mechanical behavior. Although the deformation in the neck is inhomogeneous down to a very fine level, the amorphous phase seems to deform via its own fashion (such as the pseudo-affine mode revealed) that exerts on the lamellar orientation until overwhelming plastic deformations of crystal occur.

Conclusion

The molecular orientations accompanying the necking process in a quenched iPP thin film are complicated in view of the macroscopic variables of deformation. Using a novel method of photogrammetry, the deformation of the amorphous phase during the necking propagation is shown to be affine on the mesoscale of several hundred microns; i.e., f_{am} changes with the longitudinal extension ratio $\lambda(t)$ obeying the theoretical prediction. The anisotropic shrinkage in the film width and thickness directions illuminates further this pseudo-affine behavior in iPP film differing from the pure affine deformation of true elastomers. A linear relationship between f_c and f_{am} is found to hold as far as the plastic deformation components are not dominant in a local area under examination, suggesting a lamellar orientation determined by the deformation of the amorphous chains. The proportionality constant between f_c and f_{am} is found to be 1.85 for all microcrystalline iPP film specimens tested. Applicability of this numerical value should be examined for more inhomogeneous iPP sample that contains giant spherulites as well as other semicrystalline polymers.

Acknowledgment. This work has been partially supported by the Grant-in-Aid for the Scientific Research from Ministry of Education, Culture, Sports, Science and Technology, Japan (No. 10305070) and one of the authors, Y. Song, is grateful to JSPS for the Grant-in-Aid for JSPS Fellows relating to JSPS Fellowship for Foreign Researchers (No. 12000317).We are grateful to Dr. H. W. Siesler for his helpful suggestions.

References and Notes

(1) Lu, J.; Ravi-Chandar, K. *Int. J. Solids Struct.* **1999**, *36*, 391.
(2) Tomita, Y. *Int. J. Mech. Sci.* **2000**, *42*, 1455.
(3) Ferreiro, V.; Pennec, Y.; Seguela, R.; Coulon, G. *Polymer* **2000**, *41*, 1561.
(4) Castelein, G.; Coulon, G.; G'Sell, C. *Polym. Eng. Sci.* **1997**, *37*, 1694.
(5) Li, J. X.; Cheung, W. L.; Chan, C. M. *Polymer* **1999**, *40*, 3641.
(6) Flory, P. J.; Yoon, D. Y. *Nature (London)* **1978**, *272*, 226.
(7) Gent, A. N.; Madan, S. *J. Polym. Sci., Polym. Phys. Ed.* **1989**, *27*, 1529.
(8) Shadrake, L. G.; Guiu, F. *Philos. Mag.* **1976**, *34*, 565.
(9) O'Kane, W. J.; Young, R. J.; Ryan, A. J. *J. Macromol. Sci., Phys. B* **1995**, *34*, 427.
(10) Crist, B.; Fisher, C. J.; Howard, P. R. *Macromolecules* **1989**, *22*, 1709.
(11) O'Kane, W. J.; Young, R. J. *J. Mater. Sci., Lett.* **1995**, *14*, 433.
(12) Pae, K. D.; Morrow, D. R.; Chen, Y. *Advances in Polymer Science and Engineering*; Plenum Press: New York, 1972.
(13) Hay, I. L.; Keller, A. *Kolloid Z.* **1965**, *204*, 43.
(14) Hay, I. L.; Keller, A. *J. Mater. Sci.* **1966**, *1*, 41.
(15) Hay, I. L.; Keller, A. *J. Mater. Sci.* **1967**, *2*, 538.
(16) Young, R. J. *Mater. Forum* **1988**, *11*, 210.
(17) Krupenkin, T. N.; Taylor, P. L. *Macromol. Theory Simul.* **1998**, *7*, 119.
(18) Karger-Kocsis, J.; Moskala, E. J.; Shang, P. P. *J. Therm. Anal. Calorim.* **2000**, *63*, 671.

(19) Zhou, H. Y.; Wilkes, G. L. *J. Mater. Sci.* **1998**, *33*, 287.
(20) Gordeev, S. A.; Nikolaeva, G. Y.; Prokhorov, K. A. *Vysokomol. Soedin.* **1996**, *38*, 820.
(21) Sheiko, S. S.; Kunz, M.; Moller, M. *Vysokomol. Soedin.* **1993**, *35*, 1903.
(22) Moginger, B.; Lutz, C.; Polsak, A.; Muller, U. *Colloid Polym. Sci.* **1991**, *269*, 535.
(23) Sawczuk, A.; Bianchi, G. *Plastic Today*; Elsevier Applied Science: Amsterdam, 1985.
(24) Oliey, R. H.; Bassett, D. C. *J. Macromol. Sci., Phys. B* **1994**, *33*, 209.
(25) Hutchinson, J. W.; Neale, K. W. *J. Mech. Phys. Solids* **1983**, *31*, 405.
(26) Neale, K. W.; Tugcu, P. *J. Mech. Phys. Solids* **1985**, *33*, 323.
(27) Tomita, Y.; Hayashi, K. *Int. J. Solids Struct.* **1993**, *30*, 225.
(28) Masud, A. *Int. J. Numer. Methods Eng.* **2000**, *47*, 1887.
(29) Haward, R. N. *J. Polym. Sci., Part B: Polym. Phys.* **1995**, *33*, 1481.
(30) Gaucher-Miri, V.; Francois, P.; Seguela, R. *J. Polym. Sci., Part B: Polym. Phys.* **1996**, *34*, 1113.
(31) Francois, Ph.; Gaucher, V.; Seguela, R. *J. Phys.: Condens. Matter* **1994**, *6*, 8959.
(32) Onogi, S.; Asada, T.; Takaki, T. *J. Soc. Mater. Sci. Jpn.* **1967**, *16*, 746.
(33) Mackenzie, M. W. *Advances in Applied Fourier Transformation Infrared Spectroscopy*; John Wiley & Sons: New York, 1988.
(34) Bayer, G.; Hoffmann, W.; Siesler, H. W. *Polymer* **1980**, *21*, 235.
(35) Oderkerk, J.; Groeninckx, G.; Soliman, M. *Macromolecules* **2002**, *35*, 3946.
(36) Shigematsu, Y.; Takada, A.; Nemoto, N.; Nitta, K. *Rev. Sci. Instrum.* **2001**, *72*, 3927.
(37) Song, Y.; Shigematsu, Y.; Nitta, K.-H.; Nemoto, N. *Polym. J.* **2002**, *34*, 584.
(38) Caldas, V.; Brown, G. R.; Nohr, R. S.; Macdonald, J. G.; Raboin, L. E. *Polymer* **1994**, *35*, 899.
(39) Martorana, A.; Piccarolo, S.; Sapoundjieva, D. *Macromol. Chem. Phys.* **1999**, *200*, 531.
(40) Piccarolo, S. *J. Macromol. Sci., Phys. B* **1992**, *31*, 501.
(41) Tanaka, H.; Fujiwara, Y.; Asano, T.; Polizzi, S. *Macromol. Chem. Phys.* **1993**, *194*, 2279.
(42) Ran, S. F.; Zong, X. H.; Fang, D. F.; Hsiao, B. S.; Chu, B.; Phillips, R. A. *Macromolecules* **2001**, *34*, 2569.
(43) Siesler, H. W. *Adv. Polym. Sci.* **1984**, *65*, 1.
(44) Samuels, R. J. *Makromol. Chem. Suppl.* **1981**, *4*, 241.
(45) Snyder, R. G.; Schachtschneider, J. H. *Spectrochim. Acta* **1964**, *20*, 853.
(46) Waterman, H. A. *Kolloid Z.* **1963**, *192*, 9.
(47) Viville, P.; Daoust, D.; Jonas, A. M.; Nysten, B.; Legras, R.; Dupire, M.; Michel, J.; Debyas, G. *Polymer* **2001**, *42*, 1953.
(48) Kuhn, W.; Grun, F. *Kolloid Z.* **1942**, *101*, 248.
(49) Treloar, R. L. G. *The Physics of Rubber Elasticity*, 3rd ed.; Clarendon Press: Oxford, 1975.
(50) Nagai, K. *J. Chem. Phys.* **1964**, *40*, 2818.
(51) Reo, R. J.; Krigbaum, J. *Appl. Phys.* **1964**, *35*, 2215.
(52) Ries, M. E.; Brereton, M. G.; Klein, P. G.; Ward, I. M.; Ekanayake, P.; Menge, H.; Schneider, H. *Macromolecules* **1999**, *32*, 4961.
(53) Lin, L.; Argon, A. S. *J. Mater. Sci.* **1994**, *29*, 294.
(54) Keller, A.; Pope, D. P. *J. Mater. Sci.* **1971**, *6*, 453.
(55) Pope, D. P.; Keller, A. *J. Polym. Sci., Polym. Phys. Ed.* **1975**, *12*, 533.
(56) Mayer, J.; Schrodi, W.; Heise, B.; Kilian, H. G. *Acta Polym.* **1990**, *41*, 363.
(57) Paul, E.; Heise, B.; Schrodi, W.; Kilian, H. G. *Prog. Colloid Polym. Sci.* **1991**, *85*, 12.
(58) Kilian, H. G.; Knechel, W.; Heise, B.; Zrinyi, M. *Prog. Colloid Polym. Sci.* **1993**, *92*, 60.
(59) Ward, I. M. *Structure and Properties of Oriented Polymers*; Applied Science Publishers: London, 1975.
(60) Ward, I. M. *Mechanical Properties of Solid Polymers;* Wiley-Interscience: London, 1971.
(61) Peterlin, A. *J. Mater. Sci.* **1971**, *6*, 490.
(62) Kestenbach, H.-J.; Petermann, J. *Polymer* **1994**, *35*, 5217.
(63) Wilchinsky, Z. W. *Polymer* **1964**, *5*, 271.
(64) Kratky, O. *Kolloid Z.* **1933**, *64*, 213.
(65) Ward, I. M. *Proc. Polym. Soc.* **1962**, *80*, 1176.
(66) Stein, R. S.; Norris, F. H. *J. Polym. Sci.* **1956**, *21*, 381.
(67) Samuels, R. J. *J. Polym. Sci., Part A* **1965**, *3*, 1741.

MA0214254